Reduced ensemble plasmon linewidths and enhanced two-photon luminescence in anodically formed high surface area Au-TiO_2 3D nanocomposites

Samira Farsinezhad,[1] Shyama Prasad Banerjee,[1] Bharath Bangalore Rajeeva,[1] Benjamin D. Wiltshire,[1] Himani Sharma,[1] Anton Sura,[1] Arash Mohammadpour,[1] Piyush Kar,[1] Robert Fedosejevs[1] and Karthik Shankar[1, 2*]

[1]*Department of Electrical and Computer Engineering, University of Alberta, 9211 - 116 St, Edmonton, Alberta, Canada T6G 1H9.*

[2]*NRC National Institute for Nanotechnology, 11421 Saskatchewan Dr NW, Edmonton, AB T6G 2M9.*

ABSTRACT: Localized surface plasmon resonances (LSPR) in TiO_2 nanorod and nanotube arrays decorated by gold nanoparticles can be exploited to improve photocatalytic activity, enhance non-linear optical coefficients and increase light harvesting in solar cells. However the LSPR typically has a low quality factor and the resonance is often obscured by the Urbach tail of the TiO_2 band gap absorption. Attempts to increase the LSPR extinction intensity by increasing the density of gold nanoparticles on the surface of the TiO_2 nanostructures invariably produce peak broadening due to the effects of either agglomeration or polydispersity. We present a new class of hybrid nanostructures containing gold nanoparticles (NPs) partially embedded in nanoporous/nanotubular TiO_2 by performing the anodization of co-sputtered Ti-Au thin films containing a relatively high ratio of Au:Ti. Our method of anodizing thin film stacks containing alternate layers of Ti and TiAu results in very distinctive LSPR peaks with quality factors as high as 6.9 and ensemble linewidths as small as 0.33 eV even in the presence of an Urbach tail. Unusual features in the anodization of such films are observed and explained, including oscillatory current transients and the observation of coherent hetero-interfaces between the Au

NPs and anatase TiO_2. We further show that such a plasmonic NP-embedded nanotube structure dramatically outperforms a plasmonic NP-decorated anodic nanotube structure in terms of the extinction coefficient, and achieves a strongly enhanced two-photon fluorescence due to the high density of gold nanoparticles in the composite film and the plasmonic local field enhancement.

KEYWORDS: electrochemical anodization, titania nanotubes, heterogeneous catalysis, internal electric fields, solar fuels, nonlinear optical media.

1. INTRODUCTION

The anatase phase of TiO_2 is a versatile large bandgap semiconductor prominently employed in a range of catalytic, optical, electronic and optoelectronic applications.[1-3] Consequently, there exists a strong motivation to construct nanostructured TiO_2–noble metal composites that can provide a LSPR-induced improvement in function and performance in devices such as dye-sensitized solar cells, ordered bulk heterojunction photovoltaics, photocatalysts and optical sensors through the enhancement of local electromagnetic fields and is therefore a much pursued objective.[4-12] The use of noble metal-semiconductor hybrid substrates in matrix-assisted laser desorption and ionization- time of flight (MALDI-TOF) mass spectrometry is receiving increasing attention for integration with surface enhanced Raman scattering (SERS)[13] and also for obtaining a plasmonic enhancement of molecular yields while reducing interference from large proteins.[14] A much less widely studied application is the generation of substrates for nonlinear plasmonics.

The conventional methods of decorating high surface area metal oxide nanotube and nanorod arrays by gold nanoparticles are (i) vacuum deposition followed by thermal dewetting[15] (ii) photocatalytic deposition[16] (iii) thermal decomposition of surface-adsorbed gold salts[17] (iv)

surface anchoring of colloidal Au NPs[18] and (v) various wet impregnation techniques.[19] The maximum achievable LSPR extinction coefficients per unit film thickness are limited in the conventional method of noble metal decoration by polydispersity and agglomeration, due to which weak and/or broadened resonances partially obscured by the Urbach absorption tail of TiO_2 are seen,[20-21] instead of the sharp and distinct LSPR peaks observed for Au NPs in aqueous solutions. Even when the Au nanoparticles are used to decorate photonic crystal-like periodic TiO_2 nanotube arrays, extremely broad or indistinct LSPR peaks were still observed in the optical spectra.[22-23] Because the quality factor of the LSP resonance is inversely proportional to the peak-width, many of the reports on high-activity Au-TiO_2 plasmonic photocatalysts that exhibit very broad resonances in their UV-Vis spectra,[24] in actuality have very small local electric field enhancements. The use of Au-doped sols and RF co-sputtering have also been used to form Au NPs completely embedded within TiO_2 thin films typically for nonlinear optics applications,[25-26] but the effective surface area of these planar film architectures is rather low thus limiting applications in surface enhanced Raman scattering (SERS), photocatalysis and sensing.

We present here a method based on electrochemical anodization of co-sputtered TiAu films that produces high surface area nanostructures simultaneously exhibiting strong and distinct LSPR peaks unobscured by the extinction of the TiO_2 nano-scaffolds. Depending on the fabrication conditions - gold nanoparticle-decorated titania nanorods, nanotubes or nanopores were obtained. We collectively term these nanostructures Anodic PLasmonic Au-TiO_2 Engineered Nanocomposites (A-PLATENs). A-PLATENs allowed us to achieve a Quality factor (Q) for the plasmonic resonance that is considerably higher than previously published reports as shown in Table 1. The A-PLATENs also exhibited a strong enhancement of the two-photon

luminescence when excited by femtosecond laser pulses at 800 nm. As we demonstrate later in this report, A-PLATENs have unique features such as the fact that the gold NPs are partially embedded in the TiO_2 and also the formation of select coherent hetero-interfaces between Au and TiO_2. Our electrochemical method of synthesis does not result in surfactant-coated Au NPs unlike purely chemical methods and shares many features with physical methods of preparation of Au NPs such as laser ablation,[27] which preclude the change in surface reactivity and undesirable modification of functional properties due to the presence of the surfactants. A-PLATENs are expected to extend the usage of TiO_2 nanotubes and nanorods in biosensing applications through enhanced fluorescence, refractive index sensitivity of the LSPR and higher conductivity in electrochemical sensors.[28-32] A number of unusual features were observed in the anodization process due to the high gold content of the co-sputtered films, which could provide key insights into the anodic synthesis of metal oxide thin films and nanostructures from high concentration mixtures of valve metals and non-valve metals. These aspects are discussed in more detail in the Results and Discussion section.

Table 1. Champion Q-factors obtained for the LSPR peaks in one-dimensional TiO_2 nanostructures decorated by gold nanoparticles

Reference	Type of nanostructure	Method of Au NP decoration	LSPR peak wavelength (nm)	Plasmon Resonance Energy (eV)	FWHM (eV)	LSPR Q-factor
This work	Au NP-decorated TiO_2 nanorods, nanotubes and nanopores	Electrochemical anodization of co-sputtered Au-Ti thin films	533	2.3253	0.337	6.9
Y.-C. Pu *et al, Nano Lett.* (2013)[33]	Au NP-decorated TiO_2 nanowires	Immersion in $HAuCl_4$ and calcination at 300	541	2.2940	*0.72	~3.2

Y. Tian, T. Tatsuma, *J. Am. Chem. Soc.* (2005) [34]	TiO_2 film loaded with Au NPs	Photocatalytic deposition in a porous TiO2 film	560	2.2148	1.03	~2.2
Z. Bian *et al, J. Am. Chem. Soc.* (2014)[35]	TiO_2 mesocrystals modified with Au NPs	Deposition-precipitation, followed by centrifuge and evaporation	539	2.3022	0.92	~2.5
J. Thomas, M. Yoon, *Appl. Cat. B: Env.* (2012)[36]	TiO_2 nanofibers doped with Au NPs	Hydrothermal reaction and sonication with Au NPs	552	2.2447	0.56	~4.0
Y. Wen *et al, Nanoscale* (2013)[37]	Anatase/rutile mixed TiO_2 nanotubes precipitated with Au NPs	Deposition-precipitation with $HAuCl_4$ and urea	559	2.2173	0.86	~2.6
Z. Jin *et al, ACS Appl. Mater. Interfaces* (2016)[23]	Au NP-decorated monolayer TiO_2 nanotubes	Anodic oxidation and photoreduction of $HAuCl_4$	582	2.1292	0.80	~2.7
A. Zhu *et al, Anal. Chem.* (2009)[38]	Au NPs deposited on TiO_2 nanoneedle film	12-15h immersion in Au NP suspension	539	2.2997	0.51	~4.5
S.T. Kochuveedu *et al, J. Phys. Chem. C* (2012)[39]	TiO_2 nanospheres decorated by Au NPs	TiO2 beads dispersed in citrate-capped Au NP solution	535	2.3458	0.64	~3.7
Z. Zhang *et al, J. Phys. Chem. C* (2013)[40]	TiO_2 nanofibers decorated by Au NPs	Electrospinning with postcalcination using $HAUCl_4$	574	2.1619	0.46	~4.7
A. Primo *et al, Phys. Chem. Chem.*	Titania supported gold nanoparticles	Sol-gel based thin films decorated	539	2.2988	0.75	~3.1

Phys.(2011)[41]		by spin-coating				
Y. Chen *et al, Dalton Trans.* (2012)[42]	Au-decorated TiO_2 nanotube arrays	Deposition of Au seeds in $HAuCl_4$ and *in situ* seed growth	504	2.4583	0.41	~6.0
S. Luo *et al, Sep. Pur. Tech.*(2011)[43]	Gold nanotubes consisting of Au NPs embedded in TiO_2 nanotube arrays	Electrodeposition of Au NPs using $HAuCl_4$	516	2.4032	0.66	~3.6
A.G. Dosado *et al, J. Catalysis*. (2015)[44]	Au NPs deposited on TiO_2 nanorod supports	Deposition-precipitation with urea using $HAuCl_4$	558	2.2233	0.46	~4.8
R. Ma *et al, J. Am. Chem. Soc.* (2004)[45]	Au nanocrystal-loaded titanate nanotube suspension	Reduction of nanotubes in $HAuCl_4$	521	2.3801	0.51	~4.7
L. Bu *et al, RSC Adv.* (2015)[46]	Au NPs deposited on TiO_2 single crystal nanorods	Photocatalytic reduction of $HAuCl_4$ by the nanorods	507	2.4455	0.93	~2.6

2. RESULTS AND DISCUSSION

There is one prior report of anodizing Ti-Au bimetallic composites. Schmuki and colleagues fabricated TiO_2 nanotubes decorated with 5 nm Au nanoparticles by the electrochemical anodization of Ti-Au alloy foils containing 0.02 at%, 0.2 at%, and 1 at% Au.[47] They reported high activity for photocatalytic H_2 production from ethanol solutions but did not report optical spectra for the Au NP-decorated nanotubes perhaps because their substrates were opaque. Our report differs from the aforementioned paper in a number of ways - we use bimetallic films with much higher gold content (typically 4-5 atom % of Au), we form the Ti-Au films by sputtering,

we use a multilayer film stack containing alternate layers of undoped- and Au-doped Ti instead of a homogeneously doped Au-Ti film (see Figure 1b) and we collect optical spectra which are of paramount importance in this report. Through a series of experiments, we determined that homogeneously doped Au-Ti films were unsuitable because the less reactive gold inhibited field assisted oxidation and etching for mild anodization conditions (low anodization voltage and low fluoride content in electrolyte), and was leached away by the electrolyte for stronger anodization conditions. On the other hand, we found an alternating film stack (Figure 1a) to both retain gold and generate a nanostructured anodic oxide provided that the both the initial and terminal films in the stack were undoped Ti films.

A distinctive feature of the anodization of the alternating Ti/Ti-Au film stack is the observation of oscillations in the anodization current (Figure 1d) with the number of current maxima corresponding to the number of Au-doped Ti layers. This is in contrast to the regular anodization of Ti where a single peak in the current is typically observed. Two other differences are (i) the amplitude of the current maxima for the Ti/Ti-Au film stack is much higher than that observed for the anodization of Ti foils and films and (ii) the current minima are roughly constant or at least non-decreasing until the last maximum passes. When the anodic process begins, the top-most Ti layer is first subjected to anodization and the current drops due to the formation of an insulating TiO_2 barrier layer. At this point, chemical- and field-assisted etching of the barrier layer re-open conduction paths in the barrier layer leading to the more conductive Ti-Au layer underneath and thus resulting in the current increasing. In the Ti-Au layer, Ti transforms to TiO_2 while Au nanoparticles are formed in tight bands (see Figure 1c) with significant diffusion into the surrounding regions, particularly nearly the top of the film stack. Au is not anodized and consequently, as the field-assisted oxidation process for the second undoped

Ti layer proceeds to completion, the anodization current decreases again producing a peak (the first current maximum). Likewise, current maxima are produced corresponding to the anodic oxidation of each of the undoped Ti layers below the surface layer. Due to the diffusion of the gold into the surrounding regions, the conductivity of the anodized film stack, as a whole, is higher than that of a regular TiO_2 barrier layer and accounts for the plateauing of the current minima in Figure 1d. Figure 2 shows the morphologies of the Au-TiO_2 nanocomposites obtained subsequent to anodization of the multilayer film stacks shown in Figure 1b in EG-based electrolytes containing fluoride ions.

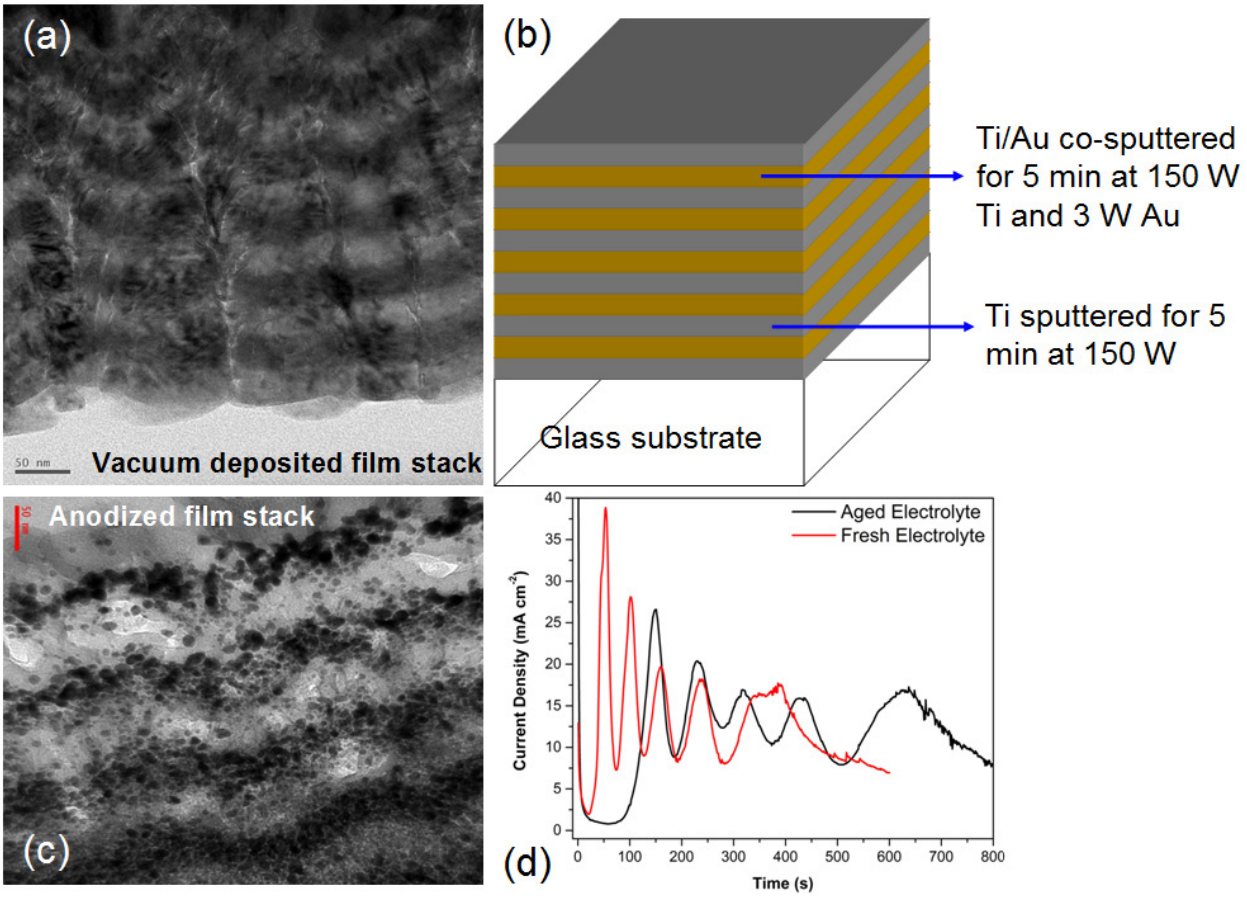

Figure 1. (a), (b) TEM cross-sectional image and schematic illustration of the thin film stack formed by sputtering alternate layers of Ti and Au-Ti on a glass substrate; (c) TEM image following anodization of the thin film stack showing bands of gold nanoparticles concentrated in regions corresponding to the Au-Ti layers

and (d) current transients recorded during the electrochemical anodization of the film stack at 40 V in an ethylene glycol-based electrolyte containing F^- species. An electrolyte used for the very first time to perform anodization is :fresh" while if the electrolyte has been previously used to perform anodization, and therefore contains $(TiF_6)^{2-}$ ions from the anodization process, then the electrolyte is "aged".

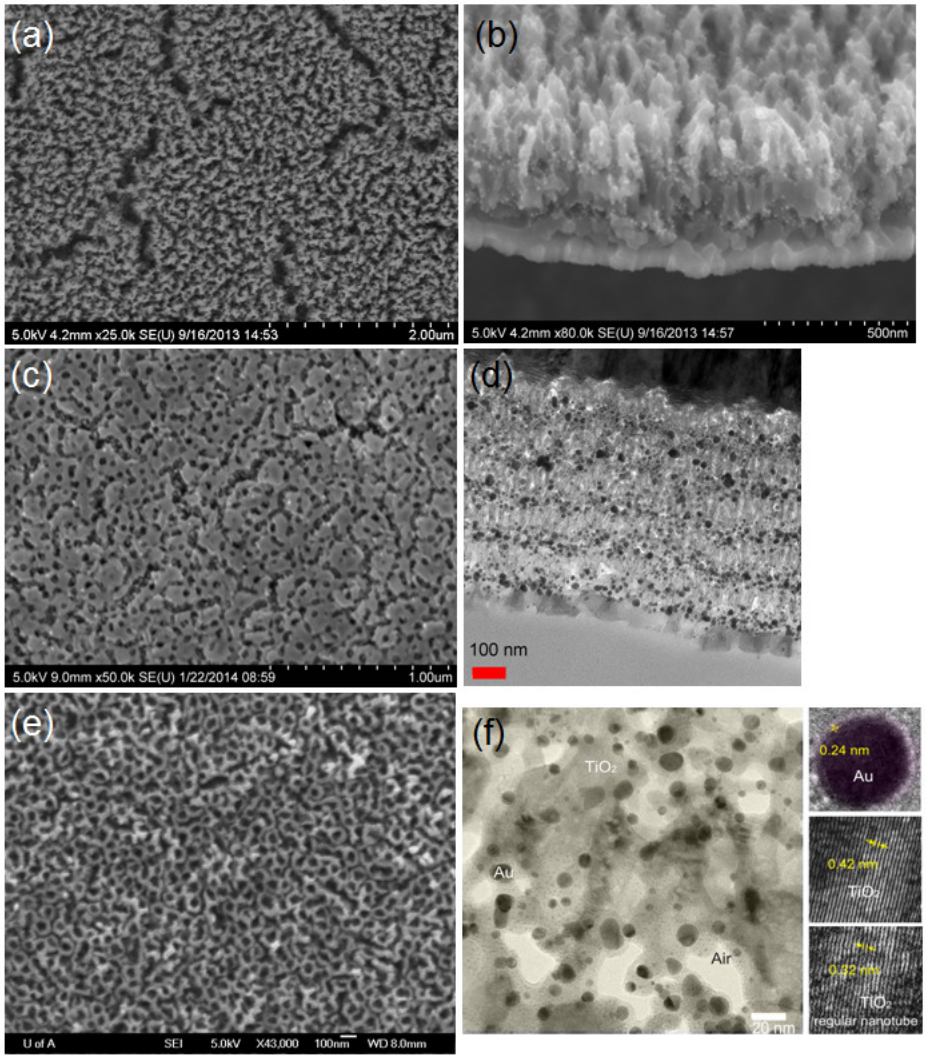

Figure 2. A-PLATEN morphologies obtained: (a, b) FESEM top-view and cross-sectional image of Au NP-decorated TiO_2 nanorod arrays formed by anodizing a thin film stack identical to that shown in Figure 1; (c, d) The anodization was performed potentiostatically at 40 V in an EG-based electrolyte containing 2 % H_2O and 0.3 % NH_4F (c) FESEM top-view and cross-sectional TEM image of Au NP-decorated TiO_2 nanorod arrays with a ~200 nm-thick nanoporous capping layer formed by anodizing a thin film stack identical to that shown

in Figure 1; The anodization was performed potentiostatically at 40 V in an EG-based electrolyte containing 1 % H_2O and 0.1 % NH_4F; the total Au content in the thin film stacks used to prepare the samples shown in (a) through (d) was 4.1 % (e) FESEM top-view of nanotube arrays formed by anodizing a thin film stack containing a smaller amount of Au in the Au-doped Ti layers. The total Au content in the deposited film was 1.4 %; (f) HRTEM image of sample in (a) showing the lattice spacings of the TiO_2 host and the Au NPs.

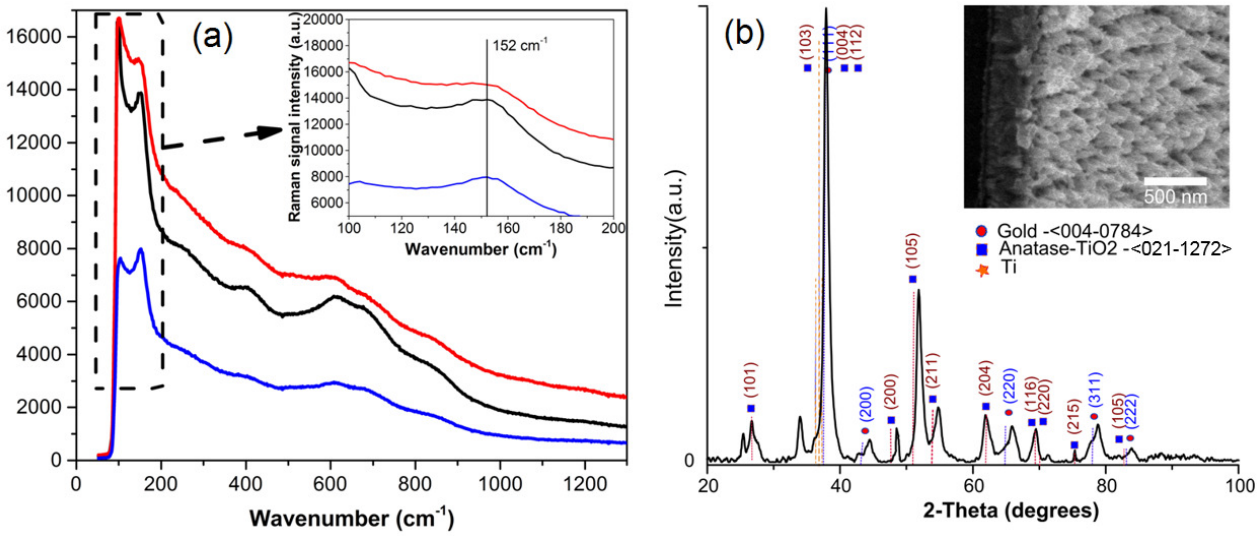

Figure 3. (a) Raman spectra of A-PLATEN formed by anodizing a thin film stack at 40 V in an EG based electrolyte containing 2 % water. The black, red and blue curves correspond to ammonium fluoride concentrations in the anodization electrolyte of 0.1 %, 0.2 % and 0.3 % respectively and the inset is a magnified view of the spectra region from 100 cm^{-1} to 200 cm^{-1} (b) X-ray diffractogram of A-PLATEN formed by anodizing a thin film stack identical to that shown in Figure 1; the inset shows a cross-sectional FESEM image of the sample showing the nanorod structures.

The Raman spectra of the films resulting from the anodization of the TiAu thin film stack following annealing are shown in Figure 3a. The anatase E_g absorption mode that normally occurs at 144 cm^{-1} is shifted by 8 cm^{-1} to higher energies (see inset of Figure 3), consistent with a previous report for Au-doped mesoporous TiO_2.[48] The higher degree of disorder in the anatase crystal structure that produces the 8 cm^{-1} positive peak shift indicates that the Au NPs do not

merely decorate the titania nanotubes but are partially embedded within them. Likewise, the B_{1g} mode of anatase (397 cm^{-1})[49] is blue-shifted to 402 cm^{-1} in the A-PLATEN. The presence of a peak at 612 cm^{-1} in Figure 3 may be indicative of the presence of a small amount of rutile whose A_{1g} mode typically occurs as a major peak at 610 cm^{-1}. A minor peak in Figure 3 at 836 cm^{-1} is attributed to the B_{2g} mode of rutile.[49] These observations find strong support in the X-ray diffractogram of the same type of sample in Figure 3b wherein several of the peaks corresponding to the anatase phases are slightly shifted from their regular positions, which we attribute to disorder and stress due to the gold doping.

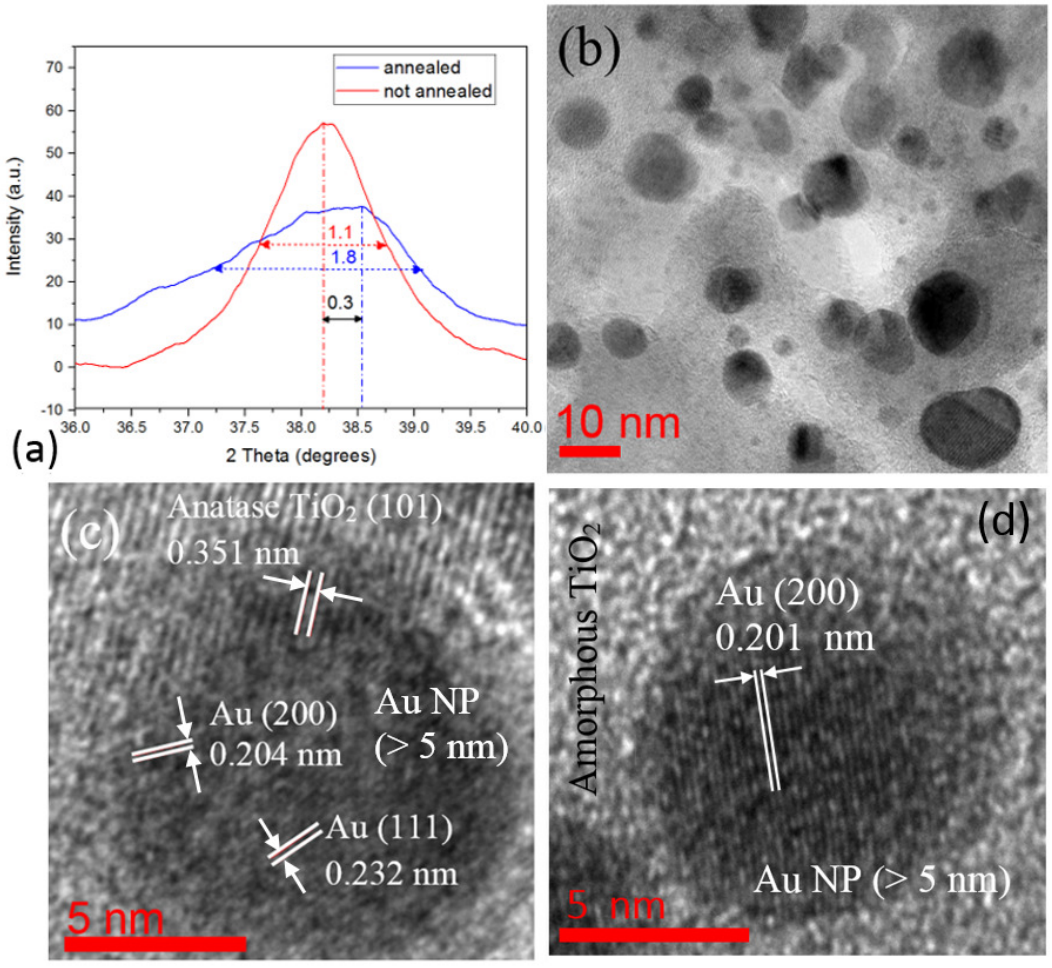

Figure 4. (a) XRD peak of the Au (111) in the Au-TiO_2 in pre- and post-annealing states; (b) Low magnification TEM image showing Au NPs in the annealed A-PLATEN; (c) and (d) HRTEM lattice fringe images of the Au NPs in annealed and un-annealed A-PLATENs respectively.

It is known that anodization of Ti in EG-based electrolytes containing 1-2 % HF results in TiO_2 nanotube arrays with a strong crystallographic texture oriented to the (004) plane of anatase subsequent to thermal annealing.[50] The X-ray diffractogram in Figure 3b indicates this to be the case even for the anodization of Ti-Au thin film stacks. Applying Scherrer's equation[51] to the Au (111) XRD peaks in Figure 4a, a post-annealing average Au NP size of 8.26 nm and a pre-annealing average Au NP size of 13.51 nm were obtained. The TEM lattice spacing of 0.351 nm in Figures 4c and 4d is consistent with the (110) reflection of anatase TiO_2.[52] Au NPs of two size regimes, i.e. smaller and larger than 5 nm, are observed in the Au-TiO_2 3D nanocomposites (Figures 4b, 4c and 4d). TEM lattice images of the larger Au nanoparticles (Figure 4c), indicate more than one facet, Au (111) and Au (200), in the annealed Au NPs. In contrast TEM lattice images of smaller Au NPs (Figure 4d) show Au (111) as the only facet. The smaller size and positive shift in the Bragg angle of about 0.3° in the post-annealed Au NPs (Figure 4a) imply a compressive stress in the post-annealed Au NPs when compared with the same before annealing.

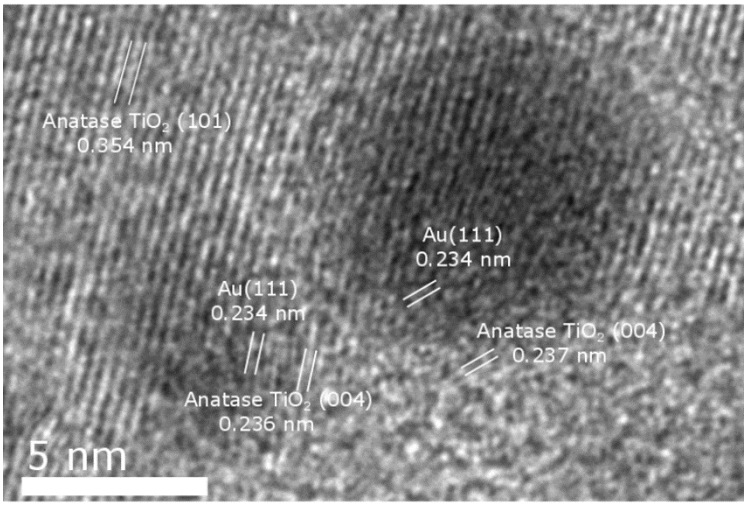

Figure 5. HRTEM image of Au-TiO_2 interface illustrating the coherent heterointerface between Au (111) and TiO_2 (004) that support the Au NPs in the TiO_2 lattice.

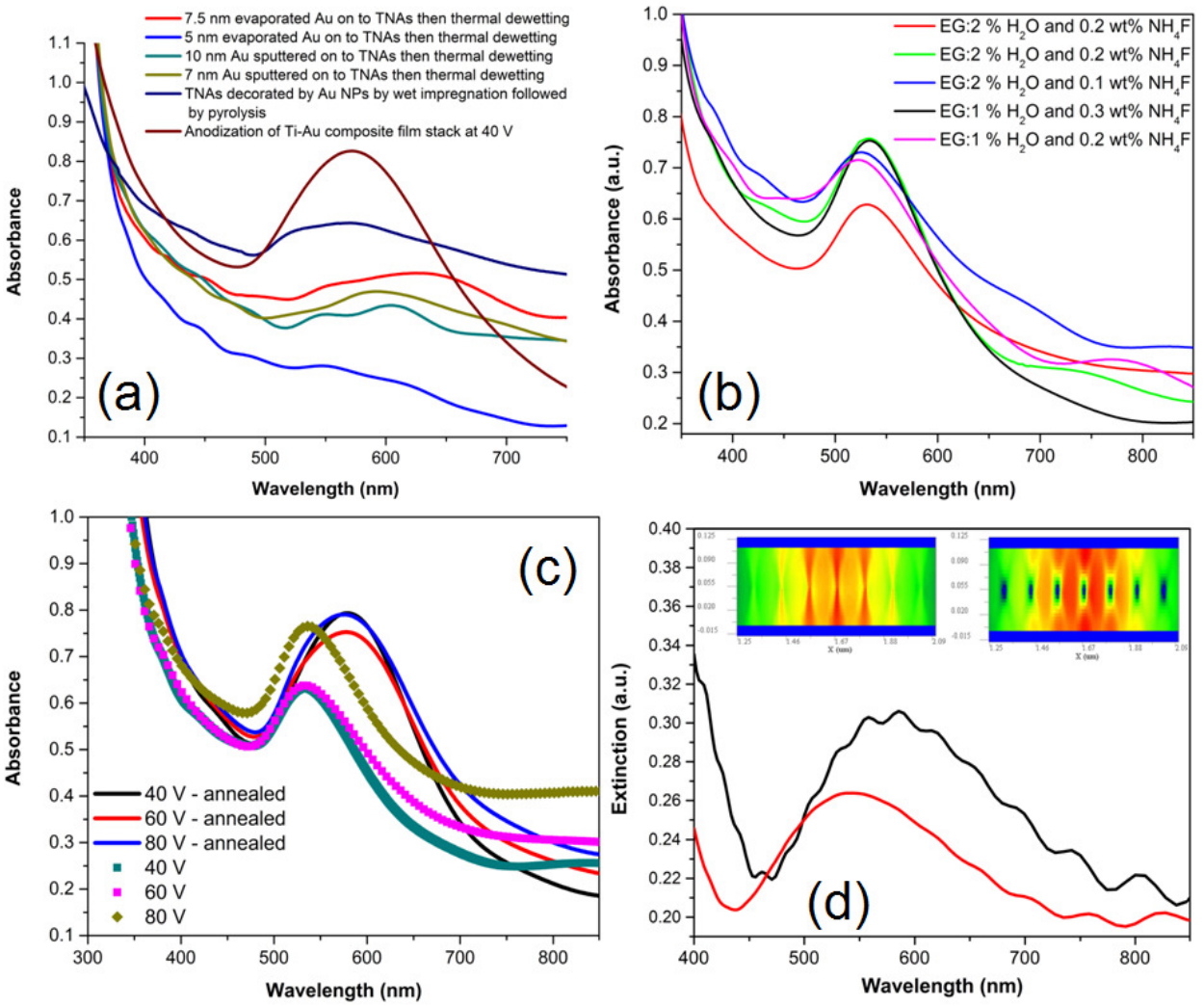

Figure 6. (a) Comparison of the optical spectra of A-PLATENs formed by anodizing a thin film stack at 40 V using an unoptimized recipe with anodic TiO_2 nanotube array samples decorated with Au NPs using other methods such as wet impregnation and vacuum deposition followed by dewetting (b) A-PLATENs formed by using electrolyte recipes optimized to achieve sharper resonances (c) Effect of anodization voltage and post-anodization thermal annealing on the LSPR peak of Au NP-decorated TiO_2 nanorod arrays and (d) Optical spectra of Au NP-decorated TiO_2 nanotube arrays from FDTD simulations; the black curve corresponds to Au NPs wedged between adjacent nanotubes with no air gaps while the red curve accounts for a finite air gap

between the Au NPs and the nanotube wall, and the insets show the magnitude of the simulated Poynting vector off-resonance (left) and at resonance (right).

Supporting Information Figure S4 indicates that Au NPs are not present in the as-deposited Au-Ti thin film stack. Larger Au NPs in the anodized and annealed A-PLATENs show secondary fringes (observed in Figure 4c) due to various grain orientations. This is in contrast with the smaller Au NPs (less than 5 nm), where the grain orientations are more uniform with a single crystal plane. The observed variance in lattice orientations of larger Au NPs are likely due to their gradual displacement or rotation, which occurs as the Au NP accommodates to stresses in the TiO_2 matrix.[53] We found evidence of coherent Au-TiO_2 heteroepitaxial interfaces for a portion of the Au NPs, as evident from quasi-matching lattices (Figure 5) of the Au (111) and anatase TiO_2 (112) crystal planes. The angle between crystal planes in the tetragonal Bravais lattice of anatase titania is given by

$$\cos\phi = \frac{\left(\frac{h_1h_2 + k_1k_2}{a^2}\right) + \left(\frac{l_1l_2}{c^2}\right)}{\sqrt{\frac{h_1^2 + k_1^2}{a^2} + \frac{l_1^2}{c^2}}\sqrt{\frac{h_2^2 + k_2^2}{a^2} + \frac{l_2^2}{c^2}}} \qquad (1)$$

The HRTEM image in Supporting Information Figure S7 shows an angle of 51.9° between the Au NP's (111) and anatase TiO_2's (100) crystal planes which have *d*-spacings of 0.237 nm and 0.372 nm respectively in the A-PLATENs. Since the (112) plane of anatase is also at an angle of 52° from the (100) anatase plane, the (112) and (111) crystal planes of gold and anatase respectively are most likely to be parallel and a planar heteroepitaxial interface is indicated. While coherent hetero-interfaces between gold nanoparticles and anatase nanostructures remain uncommon, the heteroepitaxy of Au on TiO_2 has been reported in a handful of reports.[53-56]

When we began studying Au-TiO_2 nanostructures formed by the anodization of TiAu thin film stacks, it was evident early on that these samples exhibited unusually intense LSPR bands in comparison to nanotube and nanorod array thin films of similar thickness that were decorated by Au NPs by more conventional methods such as wet impregnation, photocatalytic reduction of Au salts, vacuum deposition followed by thermal dewetting, etc. This comparison is made graphically in Figure 6a. Subsequently, we tuned the parameters of the anodization process in order to maximize the quality factor of the LSPR peak. During this process, we found that the water content and fluoride content in the electrolyte were key factors that enabled control of the full-width at half maximum (FWHM) of the LSPR peak (Figure 6b) while the anodization potential did not exercise a significant influence on the peak width (Figure 6c). The sharpest resonances were achieved using EG-based electrolytes containing 1 % H_2O and 0.3 wt % NH_4F, and 2 % H_2O and 0.2 wt % NH_4F. Figure 4c also shows that the induction of crystallinity through a high temperature anneal does affect the optical spectra significantly, red-shifting the peak wavelength by ~45 nm from 535 nm to 580 nm. HRTEM imaging indicated a smaller void fraction in the annealed samples. Since the surface plasmon resonance of gold nanoparticles is extremely sensitive to the dielectric constant of the local environment, we hypothesized that in the as-anodized state, the Au NPs were mostly surrounded by air due to a more hollow structure while in the annealed state, the voids collapsed and the Au NPs were partially surrounded by, and in contact with, TiO_2 whose dielectric constant is much larger than that of air. FDTD simulations provided support for this hypothesis. Thus in Figure 6d, we observe that a model with the Au NPs directly wedged betweeen adjacent TiO_2 nanotubes has a more red-shifted LSPR band peaking at ~590 nm while a model where air gaps are present between the Au NPs and the TiO_2 nanotubes, resulted in the more commonly observed LSPR peak at ~535 nm. The

inset of Figure 6d shows the magnitude of the Poynting vector which provides a measure of the electric field intensity in the plane of the vertically oriented nanostructures (parallel to the substrate). Close to the surface plasmon resonance (plane wave simulation at 600 nm, right inset in Figure 6d), the gold nanoparticles have a large extinction cross-section and therefore the blue dots corresponding to the location of the Au nanoparticles decorating the TiO_2 nanotubes manifest much larger dimensions in the Poynting vector magnitude plot than the actual physical size of the Au NPs. On the other hand, off resonance (plane wave simulation at 660 nm, right inset in Figure 6d), the blue dots are not observable since the extinction cross-section bears more resemblance to the physical size of the Au NPs.

The quality factor (Q) of a resonator is given by the ratio of the resonance frequency to the linewidth, expressed as the full-width at half maximum (FWHM) of the corresponding peak. It is highly desirable for sensing, photocatalysis, non-linear optics and other applications for an ensemble of nanoparticles exhibiting LSPR to have a low FWHM and a high Q. For a single plasmonic nanoparticle, Q is directly proportional to the local electric field enhancement ($L(\omega)$) while the FWHM is inversely proportional to the plasmon lifetime. For an ensemble of nanoparticles, the Q represents the lower threshold of $L(\omega)$ achievable in the structure.

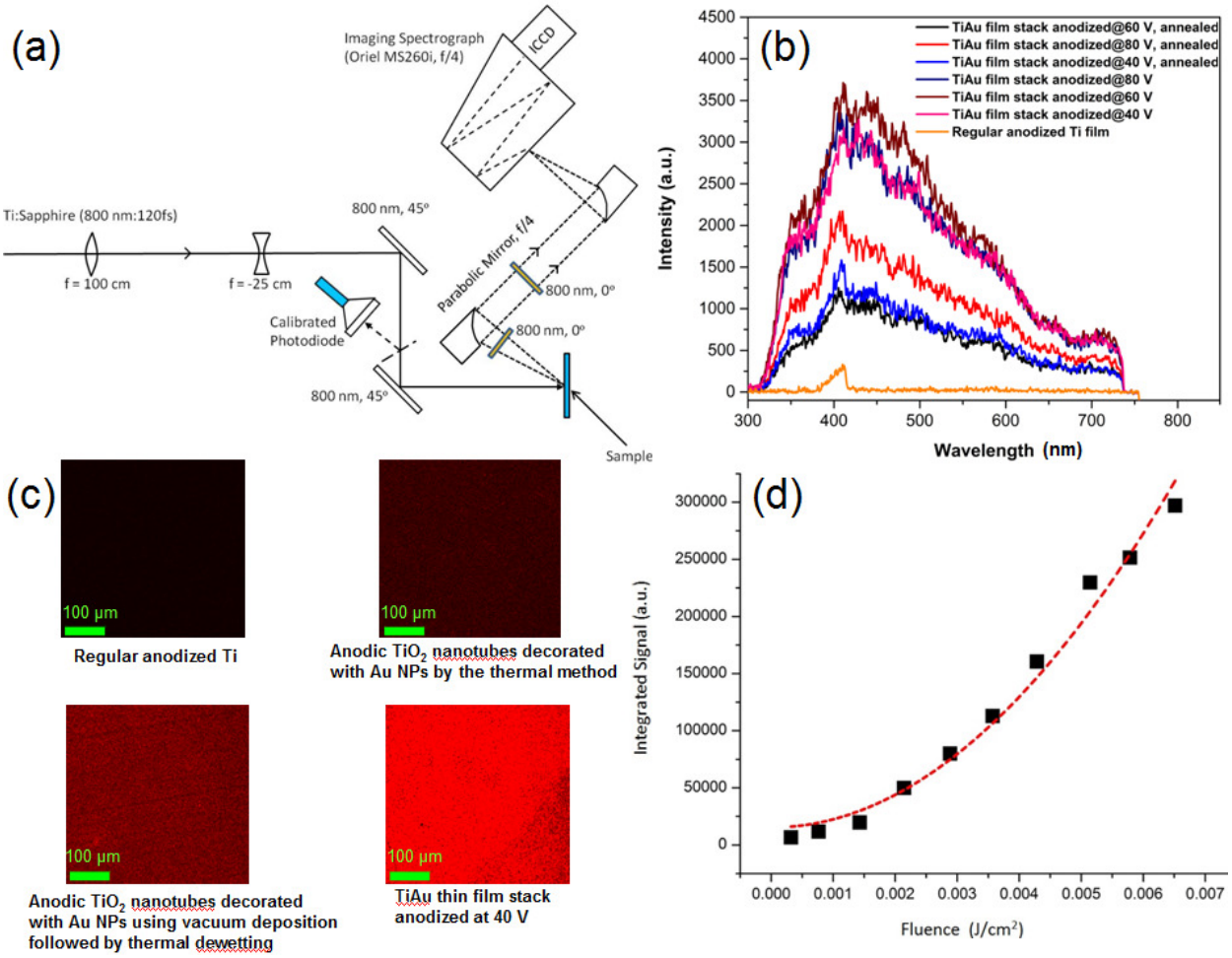

Figure 7. (a) Experimental setup used to obtain the two-photon luminescence spectra (b) Two-photon luminescence spectra obtained from A-PLATENs (c) Two-photon fluorescence images obtained in a confocal microscope using 800 nm laser excitation contrasting the enhancement obtained with A-PLATENs with regular anodic titania nanotubes as well as anodic TiO_2 nanotubes decorated with Au NPs using conventional techniques, under identical excitation and imaging conditions (d) The two-photon luminescence intensity plotted as a function of the fluence of the exciting laser for TiAu film stacks anodized at 40 V.

The measurement setup for two-photon fluorescence studies of the A-PLATENs and the resulting data obtained are shown in Figure 7. Undecorated anodically synthesized TiO_2 nanotubes exhibit a peak at ~ 400 nm (orange curve in Figure 7b, which we attribute to second harmonic generation (SHG) in the high surface area porous architecture. The SHG signal at ~400

nm of bare TiO_2 is not enhanced any more than expected from estimates of the overall surface area. Essentially, there is no local field enhancement effect for the SHG signal because the SHG peak is significantly distant in energetic terms from the LSPR. The photoluminescence quantum yield (Φ_{PL}) in smooth Au films is ~10^{-10} due to multiple non-radiative transitions and increases to 10^{-5} in 2-25 nm spherical Au NPs on account of the plasmonic enhancement of radiative transitions.[57] The PL in smooth and roughened thin films of Au has been reported to have emission peaks in two bands: 410-430 nm and 530-570 nm, which are commonly attributed to direct radiative recombination of *sp*-band electrons at the Fermi level with holes in the *d* band.[58] However, the PL in spherical Au NP suspensions was attributed to the radiative decay of particle plasmons emitted by *d*-band holes combining non-radiatively with *sp* band electrons.[57] For all the samples in this study, we observe two-photon luminescence peaks in the range 415-430 nm and 530-560 nm in addition to the SHG signal at 400 nm, consistent with prior reports but also observe a minor peak at 505 nm, whose origin is unclear to us (Supporting Information Figure S5). We also observe a shoulder at 350 nm for the A-PLATENs while the same feature is absent in the PL spectra of the TiO_2 nanotube arrays decorated by Au NPs using the wet impregnation+pyrolysis (i.e. themal) method and by using vacuum deposition followed by thermal dewetting. The most intense PL is exhibited by the as-anodized TiAu thin film stacks (un-annealed A-PLATENs) whose emission intensities are greater by a factor of 2.5-3.5 than the emission intensities of anodic TiO_2 nanotubes decorated by Au NPs using more conventional techniques. Annealing reduces the PL intensity of the A-PLATENs and also red-shifts the two major emission peaks from 415 nm to 430 nm and 535 nm to 560 nm respectively. While the intensities of the multi-photon luminescence for smooth and roughened gold films are reported to increase monotonically with increasing emission wavelength (decreasing energy),[58] the two-

photon luminescence spectra of the gold nanoparticle decorated nanostructured TiO_2 samples in this study decrease significantly at longer wavelengths. This coupled with the previously mentioned observations of a similar red-shift upon annealing in both the optical spectra and the luminescence spectra are strongly suggestive of the participation of particle plasmons in the emission process, as opposed to the purely radiative recombination of *d*-band holes with *sp*-band electrons.[57] However, systematic studies of the luminescence quantum yield as a function of the particle size are needed to confirm this suggestion, which are outside the scope of the present work.

The dependence of the integrated luminescence signal following 800 nm laser excitation was measured as a function of laser fluence, and a quadratic dependence was found within the limits of experimental error, which implies the initiation of the excitation by two-photon absorption. However the high-energy cut-off in the two-photon luminescence spectra does not occur close to 400 nm as would be expected from a process dominated purely by two-photon absroption but instead occurs at ~300 nm, limited in this case by the near-zero transmission of the laser optic below 300 nm. The combination of the emission dependence on the square of the excitation intensity coupled with a cut-off energy approaching that of three photons suggest to us that a portion of the excited states rapidly populated (fs) by two-photon absorption absorb a third photon during the reminder of the pulse duration. We therefore expect two sequential processes - two photon absorption followed by single photon absorption by the excited state.

3. CONCLUSION

We present a novel synthetic methodology to generate high surface area 3D plasmonic nanocomposites containing gold nanoparticles partially embedded in the walls of vertically

oriented TiO_2 nanorod, nanotube and nanopore arrays. The methodology consists of vacuum depositing a thin film stack consisting of alternating layers of Ti and high atom fraction Ti-Au thin films, and then anodizing the stack. The resulting 3D nanocomposite exhibits very prominent localized surface plasmon resonances with ensemble linewidths as small as 0.33 eV and *Q*-factors as high as 6.9, and also achieves a strongly enhanced two-photon photuminescence in comparison to more typical plasmonic nanostructures consisting of TiO_2 nanorod or nanotube arrays decorated with gold nanoparticles prepared through conventional vacuum- and solution-based synthetic routes. Coherent hetero-interfaces between the (112) planes of the anatase phase of TiO_2 and the (111) planes of the partially embedded gold nanoparticles were observed coupled with a more red-shifted plasmon resonance due to the higher permittivity of the TiO_2 host matrix. High surface area metal oxide-noble metal 3D nanocomposites reported here constitute a new platform to exploit plasmonic phenomena in optical and SERS sensors, in substrates for MALDI-TOF mass spectrometry and in light harvesting devices such as solar cells and photocatalysts.

ASSOCIATED CONTENT

Supporting Information. Materials and Methods, Supplementary transmission electron micrographs and 2-PL spectra peak fits. This material is available free of charge via the Internet at http://pubs.acs.org.

AUTHOR INFORMATION

Corresponding Author

* Address: Prof. Karthik Shankar, Department of Electrical & Computer Engineering, University of Alberta, Edmonton, AB, Canada. Email: kshankar@ualberta.ca

Author Contributions

S.F., H.S. and B.B.R. performed the nanomaterials growth, optical spectroscopy, and the morphological and structural studies. S.P.B. and A.M. performed the data collection and analysis for the two-photon photoluminescence spectroscopy. S.F. performed FDTD simulations. A.S. calculated Q-factors and FWHMs and compared them to prior work. B.D.W. and P.K. performed the structural analysis of the thin films and hybrid nanostructures. K.S. prepared and edited the paper. K.S. and R.F. provided guidance for the experiments.

Notes

The authors declare no competing financial interest.

ACKNOWLEDGEMENTS

This project was funded through grants from the National Research Council of Canada (NRC) and NSERC. S.F., B.D.W. and A.M. acknowledge scholarship support from Alberta Innovates Technology Futures while B.B.R. held a Canadian Commonwealth Fellowship during the conduct of this research. Some device fabrication and testing used research infrastructure made possible by a Leaders Opportunity Fund grant to K.S. from the Canada Foundation for Innovation (CFI) and the Alberta Small Equipment Grants Program (SEGP). Equipment use and staff assistance at the UofA NanoFab is acknowledged along with the funding obtained for user fees from CMC Microsystems. A.M. thanks Dr. Xuejun Sun at the Cell Imaging Facility while S.F. and P.K. thank Kai Cui at the NINT electron microscopy facility.

REFERENCES

(1) Kapilashrami, M.; Zhang, Y.; Liu, Y.-S.; Hagfeldt, A.; Guo, J. Probing the Optical Property and Electronic Structure of TiO2 Nanomaterials for Renewable Energy Applications. *Chem. Rev.* **2014,** *114,* 9662-9707.

(2) Chen, W.; Kuang, Q.; Wang, Q. X.; Xie, Z. X. Engineering a High Energy Surface of Anatase TiO2 Crystals Towards Enhanced Performance for Energy Conversion and Environmental Applications. *RSC Adv.* **2015,** *5,* 20396-20409.

(3) De Angelis, F.; Di Valentin, C.; Fantacci, S.; Vittadini, A.; Selloni, A. Theoretical Studies on Anatase and Less Common TiO2 Phases: Bulk, Surfaces, and Nanomaterials. *Chem. Rev.* **2014,** *114,* 9708-9753.

(4) Awazu, K.; Fujimaki, M.; Rockstuhl, C.; Tominaga, J.; Murakami, H.; Ohki, Y.; Yoshida, N.; Watanabe, T. A Plasmonic Photocatalyst Consisting of Silver Nanoparticles Embedded in Titanium Dioxide. *J. Am. Chem. Soc.* **2008,** *130,* 1676-1680.

(5) Standridge, S. D.; Schatz, G. C.; Hupp, J. T. Distance Dependence of Plasmon-Enhanced Photocurrent in Dye-Sensitized Solar Cells. *J. Am. Chem. Soc.* **2009,** *131,* 8407-8409.

(6) Brown, M. D.; Suteewong, T.; Kumar, R. S. S.; D'Innocenzo, V.; Petrozza, A.; Lee, M. M.; Wiesner, U.; Snaith, H. J. Plasmonic Dye-Sensitized Solar Cells Using Core-Shell Metal-Insulator Nanoparticles. *Nano Lett.* **2011,** *11,* 438-445.

(7) Liu, Z. W.; Hou, W. B.; Pavaskar, P.; Aykol, M.; Cronin, S. B. Plasmon Resonant Enhancement of Photocatalytic Water Splitting Under Visible Illumination. *Nano Lett.* **2011,** *11,* 1111-1116.

(8) Feuz, L.; Jonsson, M. P.; Hook, F. Material-Selective Surface Chemistry for Nanoplasmonic Sensors: Optimizing Sensitivity and Controlling Binding to Local Hot Spots. *Nano Lett.* **2012,** *12,* 873-879.

(9) Da, P. M.; Li, W. J.; Lin, X.; Wang, Y. C.; Tang, J.; Zheng, G. F. Surface Plasmon Resonance Enhanced Real-Time Photoelectrochemical Protein Sensing by Gold Nanoparticle-Decorated TiO2 Nanowires. *Anal. Chem.* **2014,** *86,* 6633-6639.

(10) Liu, K.; Bi, Y.; Qu, S. C.; Tan, F. R.; Chi, D.; Lu, S. D.; Li, Y. P.; Kou, Y. L.; Wang, Z. G. Efficient Hybrid Plasmonic Polymer Solar Cells with Ag Nanoparticle Decorated TiO2 Nanorods Embedded in the Active Layer. *Nanoscale* **2014,** *6,* 6180-6186.

(11) Farsinezhad, S.; Sharma, H.; Shankar, K. Interfacial band alignment for photocatalytic charge separation in TiO2 nanotube arrays coated with CuPt nanoparticles. *Phys. Chem. Chem. Phys.* **2015,** *17,* 29723-29733.

(12) Kar, P.; Farsinezhad, S.; Mahdi, N.; Zhang, Y.; Obuekwe, U.; Sharma, H.; Shen, J.; Semagina, N.; Shankar, K. Enhanced CH4 yield by photocatalytic CO2 reduction using TiO2 nanotube arrays grafted with Au, Ru, and ZnPd nanoparticles. *Nano Research* **2016,** *9,* 3478-3493.

(13) Alessandri, I.; Vassalini, I.; Bertuzzi, M.; Bontempi, N.; Memo, M.; Gianoncelli, A. "RaMassays": Synergistic Enhancement of Plasmon-Free Raman Scattering and Mass Spectrometry for Multimodal Analysis of Small Molecules. *Scientific Reports* **2016,** *6,* Art. No. 34521.

(14) Li, X.; Tan, J.; Yu, J.; Feng, J.; Pan, A.; Zheng, S.; Wu, J. Use of a Porous Silicon–Gold Plasmonic Nanostructure to Enhance Serum Peptide Signals in MALDI-TOF Analysis. *Anal. Chim. Acta* **2014,** *849,* 27-35.

(15) Nitta, S.; Yamamoto, A.; Kurita, M.; Arakawa, R.; Kawasaki, H. Gold-Decorated Titania Nanotube Arrays as Dual-Functional Platform for Surface-Enhanced Raman Spectroscopy and Surface-Assisted Laser Desorption/Ionization Mass Spectrometry. *ACS Appl. Mater. Interfaces* **2014,** *6,* 8387-8395.

(16) Yu, J. G.; Dai, G. P.; Huang, B. B. Fabrication and Characterization of Visible-Light-Driven Plasmonic Photocatalyst Ag/AgCl/TiO2 TiO2 Nanotube Arrays. *J. Phys. Chem. C* **2009,** *113,* 16394-16401.

(17) Elmoula, M. A.; Panaitescu, E.; Phan, M.; Yin, D.; Richter, C.; Lewis, L. H.; Menon, L. Controlled Attachment of Gold Nanoparticles on Ordered Titania Nanotube Arrays. *J. Mater. Chem.* **2009,** *19,* 4483-4487.

(18) Ampelli, C.; Genovese, C.; Lanzafame, P.; Perathoner, S.; Centi, G., A Sustainable Production of H-2 by Water Splitting and Photo-Reforming of Organic Wastes on Au/TiO2 Nanotube Arrays. In *Pres 2014, 17th Conference on Process Integration, Modelling and Optimisation for Energy Saving and Pollution Reduction, Pts 1-3*, Varbanov, P. S.; Klemes, J. J.; Liew, P. Y.; Yong, J. Y.; Stehlik, P., Eds. 2014; Vol. 39, pp 1627-1632.

(19) Zhu, B. L.; Sui, Z. M.; Wang, S. R.; Chen, X.; Zhang, S. M.; Wu, S. H.; Huang, W. P. Alternative Approaches to Fabrication of Gold-Modified TiO2 Nanotubes. *Mater. Res. Bull.* **2006,** *41,* 1097-1104.

(20) Sudhagar, P.; Song, T.; Devadoss, A.; Lee, J. W.; Haro, M.; Terashima, C.; Lysak, V. V.; Bisquert, J.; Fujishima, A.; Gimenez, S.; Paik, U. Modulating the Interaction Between Gold and TiO2 Nanowires for Enhanced Solar Driven Photoelectrocatalytic Hydrogen Generation. *Phys. Chem. Chem. Phys.* **2015,** *17,* 19371-19378.

(21) Xu, Z.; Lin, Y.; Yin, M.; Zhang, H.; Cheng, C.; Lu, L.; Xue, X.; Fan, H. J.; Chen, X.; Li, D. Understanding the Enhancement Mechanisms of Surface Plasmon-Mediated Photoelectrochemical Electrodes: A Case Study on Au Nanoparticle Decorated TiO2 Nanotubes. *Adv. Mater. Inter.* **2015,** *2,* Art. No. 1500169.

(22) Zhang, Z.; Zhang, L.; Hedhili, M. N.; Zhang, H.; Wang, P. Plasmonic Gold Nanocrystals Coupled with Photonic Crystal Seamlessly on TiO2 Nanotube Photoelectrodes for Efficient Visible Light Photoelectrochemical Water Splitting. *Nano Lett.* **2013,** *13,* 14-20.

(23) Jin, Z.; Wang, Q.; Zheng, W.; Cui, X. Highly Ordered Periodic Au/TiO2 Hetero-Nanostructures for Plasmon-Induced Enhancement of the Activity and Stability for Ethanol Electro-Oxidation. *ACS Appl. Mater. Interfaces* **2016,** *8,* 5273-5279.

(24) Wang, H.; You, T.; Shi, W.; Li, J.; Guo, L. Au/TiO2/Au as a Plasmonic Coupling Photocatalyst. *J. Phys. Chem. C* **2012,** *116,* 6490-6494.

(25) Li, T.; Moon, J.; Morrone, A. A.; Mecholsky, J. J.; Talham, D. R.; Adair, J. H. Preparation of Ag/SiO2 Nanosize Composites by a Reverse Micelle and Sol−Gel Technique. *Langmuir* **1999,** *15,* 4328-4334.

(26) Hernando, G.; Ramki, K.; Radhakrishna, S. Nonlinear Optical Properties of Multi-Metal Nanocomposites in a Glass Matrix. *J. Phys. B: At., Mol. Opt. Phys.* **2009,** *42,* Art. No. 175401.

(27) Intartaglia, R.; Rodio, M.; Abdellatif, M.; Prato, M.; Salerno, M. Extensive Characterization of Oxide-Coated Colloidal Gold Nanoparticles Synthesized by Laser Ablation in Liquid. *Materials* **2016,** *9,* Art. No. 775.

(28) Mun, K.-S.; Alvarez, S. D.; Choi, W.-Y.; Sailor, M. J. A Stable, Label-free Optical Interferometric Biosensor Based on TiO2 Nanotube Arrays. *ACS Nano* **2010,** *4,* 2070-2076.

(29) Liu, S.; Chen, A. Coadsorption of Horseradish Peroxidase with Thionine on TiO2 Nanotubes for Biosensing. *Langmuir* **2005,** *21,* 8409-8413.

(30) An, Y.; Tang, L.; Jiang, X.; Chen, H.; Yang, M.; Jin, L.; Zhang, S.; Wang, C.; Zhang, W. A Photoelectrochemical Immunosensor Based on Au-Doped TiO2 Nanotube Arrays for the Detection of α-Synuclein. *Chemistry – A European Journal* **2010,** *16,* 14439-14446.

(31) Kar, P.; Pandey, A.; Greer, J. J.; Shankar, K. Ultrahigh Sensitivity Assays for Human Cardiac Troponin I Using TiO2 Nanotube Arrays. *Lab Chip* **2012,** *12,* 821-828.

(32) Farsinezhad, S.; Mohammadpour, A.; Dalrymple, A. N.; Geisinger, J.; Kar, P.; Brett, M. J.; Shankar, K. Transparent Anodic TiO_2 Nanotube Arrays on Plastic Substrates for Disposable Biosensors and Flexible Electronics. *J. Nanosci. Nanotechnol.* **2013,** *13,* 2885-2891.

(33) Pu, Y. C.; Wang, G.; Chang, K. D.; Ling, Y.; Lin, Y. K.; Fitzmorris, B. C.; Liu, C. M.; Lu, X.; Tong, Y.; Zhang, J. Z.; Hsu, Y. J.; Li, Y. Au Nanostructure-Decorated TiO2 Nanowires Exhibiting Photoactivity Across Entire UV-Visible Region for Photoelectrochemical Water Splitting. *Nano Lett.* **2013,** *13,* 3817-3823.

(34) Tian, Y.; Tatsuma, T. Mechanisms and Applications of Plasmon-Induced Charge Separation at TiO2 Films Loaded with Gold Nanoparticles. *J. Am. Chem. Soc.* **2005,** *127,* 7632-7637.

(35) Bian, Z.; Tachikawa, T.; Zhang, P.; Fujitsuka, M.; Majima, T. Au/TiO2 Superstructure-Based Plasmonic Photocatalysts Exhibiting Efficient Charge Separation and Unprecedented Activity. *J. Am. Chem. Soc.* **2014,** *136,* 458-465.

(36) Thomas, J.; Yoon, M. Facile Synthesis of Pure TiO2(B) Nanofibers Doped with Gold Nanoparticles and Solar Photocatalytic Activities. *Applied Catalysis B: Environmental* **2012,** *111-112,* 502-508.

(37) Wen, Y.; Liu, B.; Zeng, W.; Wang, Y. Plasmonic Photocatalysis Properties of Au Nanoparticles Precipitated Anatase/Rutile Mixed TiO2 Nanotubes. *Nanoscale* **2013,** *5,* 9739-9746.

(38) Zhu, A.; Luo, Y.; Tian, Y. Plasmon-Induced Enhancement in Analytical Performance Based on Gold Nanoparticles Deposited on TiO2 Film. *Anal. Chem.* **2009,** *81,* 7243-7247.

(39) Kochuveedu, S. T.; Kim, D.-P.; Kim, D.-H. Surface-Plasmon-Induced Visible Light Photocatalytic Activity of TiO2 Nanospheres Decorated by Au Nanoparticles with Controlled Configuration. *J. Phys. Chem. C* **2012,** *116,* 2500-2506.

(40) Zhang, Z.; Wang, Z.; Cao, S. W.; Xue, C. Au/Pt Nanoparticle-Decorated TiO2 Nanofibers with Plasmon-Enhanced Photocatalytic Activities for Solar-To-Fuel Conversion. *J. Phys. Chem. C* **2013,** *117,* 25939-25947.

(41) Primo, A.; Corma, A.; García, H. Titania Supported Gold Nanoparticles as Photocatalyst. *Phys. Chem. Chem. Phys.* **2011,** *13,* 886-910.

(42) Chen, Y.; Tian, G.; Pan, K.; Tian, C.; Zhou, J.; Zhou, W.; Ren, Z.; Fu, H. In Situ Controlled Growth of Well-Dispersed Gold Nanoparticles in TiO2 Nanotube Arrays as Recyclable Substrates for Surface-Enhanced Raman Scattering. *Dalton Trans.* **2012,** *41,* 1020-1026.

(43) Luo, S.; Xiao, Y.; Yang, L.; Liu, C.; Su, F.; Li, Y.; Cai, Q.; Zeng, G. Simultaneous Detoxification of Hexavalent Chromium and Acid Orange 7 by a Novel Au/TiO2 Heterojunction Composite Nanotube Arrays. *Sep. Purif. Technol.* **2011,** *79,* 85-91.

(44) Dosado, A. G.; Chen, W. T.; Chan, A.; Sun-Waterhouse, D.; Waterhouse, G. I. N. Novel Au/TiO2 photocatalysts for hydrogen production in alcohol-water mixtures based on hydrogen titanate nanotube precursors. *J. Catal.* **2015,** *330,* 238-254.

(45) Ma, R.; Sasaki, T.; Bando, Y. Layer-By-Layer Assembled Multilayer Films of Titanate Nanotubes, Ag- or Au-Loaded Nanotubes, and Nanotubes/Nanosheets with Polycations. *J. Am. Chem. Soc.* **2004,** *126,* 10382-10388.

(46) Bu, L.; Yang, W.; Ming, H. Low Temperature Synthesis of Rutile TiO2 Single Crystal Nanorods with Exposed (002) Facets and Their Decoration with Gold Nanoparticles for Photocatalytic Applications. *RSC Adv.* **2015,** *5,* 45122-45128.

(47) Lee, K.; Hahn, R.; Altomare, M.; Selli, E.; Schmuki, P. Intrinsic Au Decoration of Growing TiO2 Nanotubes and Formation of a High-Efficiency Photocatalyst for H2 Production. *Adv. Mater.* **2013,** *25,* 6133-6137.

(48) Li, H.; Bian, Z.; Zhu, J.; Huo, Y.; Li, H.; Lu, Y. Mesoporous Au/TiO2 Nanocomposites with Enhanced Photocatalytic Activity. *J. Am. Chem. Soc.* **2007,** *129,* 4538-4539.

(49) Tompsett, G. A.; Bowmaker, G. A.; Cooney, R. P.; Metson, J. B.; Rodgers, K. A.; Seakins, J. M. The Raman Spectrum of Brookite, TiO2 (Pbca, Z = 8). *J. Raman Spectrosc.* **1995,** *26,* 57-62.

(50) Lee, S.; Park, I. J.; Kim, D. H.; Seong, W. M.; Kim, D. W.; Han, G. S.; Kim, J. Y.; Jung, H. S.; Hong, K. S. Crystallographically Preferred Oriented TiO2 Nanotube Arrays for Efficient Photovoltaic Energy Conversion. *Energ. Environ. Sci.* **2012,** *5,* 7989-7995.

(51) Langford, J. I.; Wilson, A. Scherrer After Sixty Years: A Survey and Some New Results in the Determination of Crystallite Size. *J. Appl. Crystallogr.* **1978,** *11,* 102-113.

(52) Powder Diffraction File Card No. 21-1272 *JCPDS-International Centre for Diffraction Data, Swarthmore* **1997**.

(53) Shibata, N.; Goto, A.; Matsunaga, K.; Mizoguchi, T.; Findlay, S.; Yamamoto, T.; Ikuhara, Y. Interface Structures of Gold Nanoparticles on TiO2 (110). *Phys. Rev. Lett.* **2009,** *102,* Art. No. 136105.

(54) Giorgio, S.; Henry, C. R.; Pauwels, B.; Van Tendeloo, G. Au Particles Supported on (110) Anatase-TiO2. *Materials Science and Engineering: A* **2001,** *297,* 197-202.

(55) Akita, T.; Tanaka, K.; Tsubota, S.; Haruta, M. Analytical High–Resolution TEM Study of Supported Gold Catalysts: Orientation Relationship between Au Particles and TiO2 Supports. *Journal of Electron Microscopy* **2000,** *49,* 657-662.

(56) Nagamatsu, D.; Nemoto, T.; Kurata, H.; Jiu, J.; Adachi, M.; Isoda, S. Interface Structure of Gold Particles on TiO2 Anatase. *Mater. Trans.* **2011,** *52,* 280-284.
(57) Dulkeith, E.; Niedereichholz, T.; Klar, T.; Feldmann, J.; Von Plessen, G.; Gittins, D.; Mayya, K.; Caruso, F. Plasmon Emission in Photoexcited Gold Nanoparticles. *Phys. Rev. B* **2004,** *70,* 205424.
(58) Boyd, G.; Yu, Z.; Shen, Y. Photoinduced Luminescence from the Noble Metals and Its Enhancement on Roughened Surfaces. *Phys. Rev. B* **1986,** *33,* Art. No. 7923.